

Toluene–water clusters: Ion fragmentation and chemistry

Shijian Li and Elliot R. Bernstein

Citation: *The Journal of Chemical Physics* **97**, 792 (1992); doi: 10.1063/1.463181

View online: <http://dx.doi.org/10.1063/1.463181>

View Table of Contents: <http://aip.scitation.org/toc/jcp/97/2>

Published by the *American Institute of Physics*



**COMPLETELY
REDESIGNED!**

**PHYSICS
TODAY**

Physics Today Buyer's Guide
Search with a purpose.

Toluene-water clusters: Ion fragmentation and chemistry

Shijian Li and Elliot R. Bernstein

Colorado State University, Chemistry Department, Fort Collins, Colorado 80523

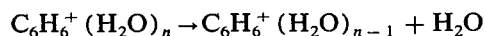
(Received 22 January 1992; accepted 30 March 1992)

Toluene/water cluster ion fragmentation is studied for isolated cold clusters by means of one- and two-color mass resolved excitation spectroscopy, time resolved pump ($S_1 \leftarrow S_0$) probe ($I \leftarrow S_1$) spectroscopy on the nanosecond time scale, and nozzle/laser delay timing experiments. These experiments lead to an identification of parent clusters for all fragment ion clusters observed. Fragmentation reactions depend on cluster size and on the energy deposited in the ion by the two photon $I \leftarrow S_1 \leftarrow S_0$ excitation sequence. Fragments identified by these techniques include $(\text{H}_2\text{O})_x \text{H}^+$ ($x = 3, \dots, 6$) and toluene $^+ (\text{H}_2\text{O})_{n-1}$ for toluene $(\text{H}_2\text{O})_n$ clusters and $(\text{H}_2\text{O})_x \text{D}^+$, $(\text{H}_2\text{O})_x \text{H}^+$, and toluene- $\text{d}_3^+ (\text{H}_2\text{O})_{n-1}$ for toluene- $\text{d}_3 (\text{H}_2\text{O})_n$ clusters. For $n \leq 3$ the preferred cluster fragmentation pathway is loss of a single H_2O molecule, while for $n \geq 4$ the preferred cluster fragmentation pathway is generation of $(\text{H}_2\text{O})_n \text{H}^+$. Cluster ion fragmentation is prevalent in this system because of product stability (i.e., solvated protons and the benzyl radical) and because the $I \leftarrow S_1$ transition leaves the cluster ion in a very highly excited vibrational state ($\Delta v \gg 0$ for the $I \leftarrow S_1$ transition). The fragmentation of toluene $^+ (\text{H}_2\text{O})_3$ to generate $(\text{H}_2\text{O})_3 \text{H}^+$ and a benzyl radical takes place by two distinct pathways with generation times $\tau_1 < 60$ ns and $\tau_2 = 480$ ns. The toluene $^+ (\text{H}_2\text{O})_2$ fragmentation from toluene $^+ (\text{H}_2\text{O})_3$ has a generation time of $\tau < 60$ ns. The possible energetics, kinetics, and mechanisms for these fragmentations are discussed.

I. INTRODUCTION

The study of clusters composed of an aromatic molecule (solute) and a number of small molecules (solvent species) is motivated by three main concerns: (1) solvation effects on isolated molecule structure and energy levels;¹ (2) energy dynamics in condensed phases (under solvation conditions) compared to energy dynamics in isolated molecules;² and (3) the effect of solvation on unimolecular and bimolecular chemistry.³ Observed cluster behavior is, in general, different for polar and nonpolar solvents. The behavior of clusters consisting of a solute molecule and nonpolar solvents is characterized typically by small shifts from isolated molecule spectra, sharp (molecularlike) ionization thresholds, no cluster fragmentation at the (apparent) ionization threshold, simple vibrational dynamics [intracluster vibrational redistribution (IVR)] and unimolecular vibrational predissociation (VP) reactions, and no evident intermolecular chemistry in any accessed electronic state (i.e., ground state, first excited singlet state, and the cluster ion ground electronic state). The behavior of clusters consisting of a solute molecule and polar solvents (e.g., NH_3 , H_2O , $R\text{OH}$, NR_3 , etc.) is quite different: broad ionization thresholds,⁴ extensive cluster fragmentation at the apparent ionization threshold,⁵ and cluster S_1 and/or ion chemistry⁶ (*vide infra*) are all quite typical.

In the extreme case, recently reported for benzene/water clusters,⁷ the ion fragmentation reaction



apparently cannot be avoided. Other more extreme examples of cluster ion chemistry can be found in the toluene/water and ammonia systems for which both the above

fragmentation reaction and reactions generating $(\text{H}_2\text{O})_n \text{H}^+$ ($n \geq 3$), and $(\text{NH}_3)_m \text{H}^+$ ($m \geq 1, n > m$) can be characterized.^{8(a)} Similar results are obtained for benzyl alcohol/water and ammonia clusters.^{8(b)} (Throughout this paper we use the letter n to signify the number of solvent molecules in the original parent cluster prior to fragmentation of the ion.)

Cluster fragmentation is particularly extensive for ionic clusters in which reactions can occur. Under these conditions, the exothermicity of the reaction as well as the energy associated with the geometry difference between neutral and ionic clusters can contribute to the fragmentation of parent clusters. Since the cluster ion chemistry of such systems is largely not explored, elucidating the cluster ion geometry, binding energies, and reactions is an important goal. The first step in this process is simply to enumerate the specific reactions occurring for the various cluster ions [e.g., toluene $^+ (\text{H}_2\text{O})_n$, $(\text{NH}_3)_n$, benzyl alcohol $(\text{H}_2\text{O})_n$, $(\text{NH}_3)_n$, etc.] generated as a function of $S_1 \leftarrow S_0$ and $I \leftarrow S_1$ excitation energy. One must know simultaneously what cluster is accessed and what are the products generated in the cluster reaction. This is often, as is typical for the study of chemical reactions, a tedious effort in which reactants, products, and energy and mass balance must be established and only subsequent to these determinations can reactions kinetics and mechanisms be addressed. The tools we use to accomplish these determinations are $S_1 \leftarrow S_0$ spectroscopic identification of the individual cluster transitions for clusters of different mass ($n = 1, 2, \dots$), variation of the ionization energy $I \leftarrow S_1$, identification of cluster fragment products in mass spectra and nozzle/laser timing delay studies.

In this report we explore the cluster ion chemistry of

toluene/water clusters. The chemistry of other cluster ions (toluene/ammonia,^{8(a)} benzyl alcohol and amine/water, and ammonia^{8(b)}) are dealt with in separate reports. The particular focus of this paper concerns four main themes: association of a given resolved spectrum with a specific cluster $C_6H_5CH_3(H_2O)_n$; identification of particular cluster ion fragmentation patterns as a function of ionization energy; demonstration that the observed chemistry does indeed occur on the ground state ion potential surface and not the S_0 , S_1 , or T_n surfaces; and association of (qualitative) cluster structure with the observed chemistry.

II. EXPERIMENTAL PROCEDURES

The reported experimental results are mass resolved excitation spectra (MRES).⁹ Both one- and two-color experiments are carried out. For one-color experiments, a single Nd/YAG pumped dye laser is employed to excite the cluster or molecule to S_1 and subsequently to ionize it, generating both the $S_1 \leftarrow S_0$ spectrum as the laser is scanned and the various fragment ion signals. The dye used in these experiments is LDS698: the fundamental output of the dye laser is doubled and mixed with the 1064 nm fundamental output of the Nd/YAG pump laser. Other experimental conditions include: helium backing pressure at 50 psi and toluene and water saturated vapor pressure maintained at $T \sim 300$ K. For two-color experiments, two separate Nd/YAG pumped dye lasers are employed, one of which induces the $S_1 \leftarrow S_0$ transition and the other induces the $I \leftarrow S_1$ transition. Both lasers can be scanned to generate "spectra" of the two different transitions. The ionization dye laser for these two-color experiments uses DCM, R640 or kiton red as the lasing medium. Scanning the ionization dye laser for a fixed excitation energy yields ionization threshold spectra. Observing the ion signal intensity as a function of time separation between the two lasers in a two-color experiment yields the lifetimes of various ion signals originating from the S_1 state.

Information about parent cluster size can additionally be obtained by noting the time delay between nozzle opening and the initial appearance of signal intensity in any given mass channel. Signals which arise from cluster fragmentation will still have a nozzle/signal time delay indicative of the parent cluster. This time delay is associated with two phenomena: (1) flow speed differences (velocity slippage) in the supersonic expansion for different masses; and (2) cluster formation within the nozzle opening time. The heavier the cluster mass the larger is the time delay between nozzle opening and maximum signal observation as velocity slippage is greater for larger masses and larger clusters are formed later in the nozzle opening sequence. While neither of these factors can be effectively predicted *a priori*, these time differences can be utilized to associate parent cluster mass with particular $S_1 \leftarrow S_0$ absorption features. In order to acquire such data, the time delay between nozzle opening and laser firing is scanned for given transitions in different mass channels and plotted on a single graph. Signals arising in different mass channels but associated with a given parent cluster will all have the same time delay with regard to nozzle and laser firing, even though their flight times in the drift tube after excitation/ionization are quite different.

III. EXPERIMENTAL RESULTS

The experimental results presented in this section consist of one- and two-color MRES, nozzle/laser time delay studies, and ionization threshold studies. The difficulty presented by this data set is that particular spectroscopic cluster features often appear in more than five different mass channels: the parent cluster associated with a given feature is thus by no means clear. The initial goal of these experiments is to determine the parent cluster for a specific identifiable spectroscopic feature.

Once the "reactant" (parent) cluster is identified, the "product" (fragment) clusters can be associated with it and the overall unimolecular chemical reactions taking place in the cluster ions can be elucidated. These reactions are, of course, a function of cluster ion energy and the energy dependence of product formation must also be determined through two-color MRES and threshold ionization studies. One- and two-color MRES data are needed to trace the various reaction and fragmentation pathways and the time delay studies can verify that groups of features have the relative time dependence appropriate for a given mass channel. The spectroscopic and time delay data sets are quite involved and required meticulous pursuit of each spectral feature through a series of mass channels and time delays. The reward for this effort is an elucidation of the cluster ion chemistry (i.e., identification of reactants, products, reaction pathways, and dynamics) of toluene(H_2O)_n. The fundamental results are summarized in Scheme I and Tables I and II. We follow the logic and detail of this process in the rest of this section.

A. One-color mass resolved excitation spectra

One-color MRES observed in mass channels appropriate for toluene(H_2O)_m ($m = 1, \dots, 4$) clusters are presented in Fig. 1(a)–1(d). Some representative features in these spectra are labeled so that one can follow their appearance in the different mass channels. The negative features in these spectra are caused by microchannel plate overload at the toluene flight time. Two vibrational progressions can be identified in the toluene(H_2O)₁ mass channel [Fig. 1(a)]: one of 7 cm^{-1} spacing and the other of 50 cm^{-1} spacing. To reveal the nature of these vibrational motions, isotopic substitution of both the toluene methyl group and the water molecules can be pursued. Deuteration of the toluene (free) methyl rotor yields no shifts of any observed cluster transitions near the 0_0^0 structure of toluene(H_2O)_m ($m = 1, \dots, 4$) clusters. Deuteration of the water to form toluene(D_2O)_m clusters yields a 6% ($\sim 0.5 \text{ cm}^{-1}$) red shift in the 7 cm^{-1} motion and less than 1% ($\sim 0.5 \text{ cm}^{-1}$) blue shift in the 50 cm^{-1} progression observed in the toluene(H_2O)₁ mass channel. Given these results one can tentatively conclude that the observed features in the toluene(H_2O)₁ mass channel are not due to methyl rotor transitions or a given water molecule rotation about its own symmetry (C_2) axis. These data [Fig. 1(a)] suggest that the generator of the spectrum observed in the toluene(H_2O)₁ mass channel may not be associated with the toluene(H_2O)₁ cluster. The pattern of this spectrum also suggests a different parent cluster geometry in the S_0 and S_1 electronic states.

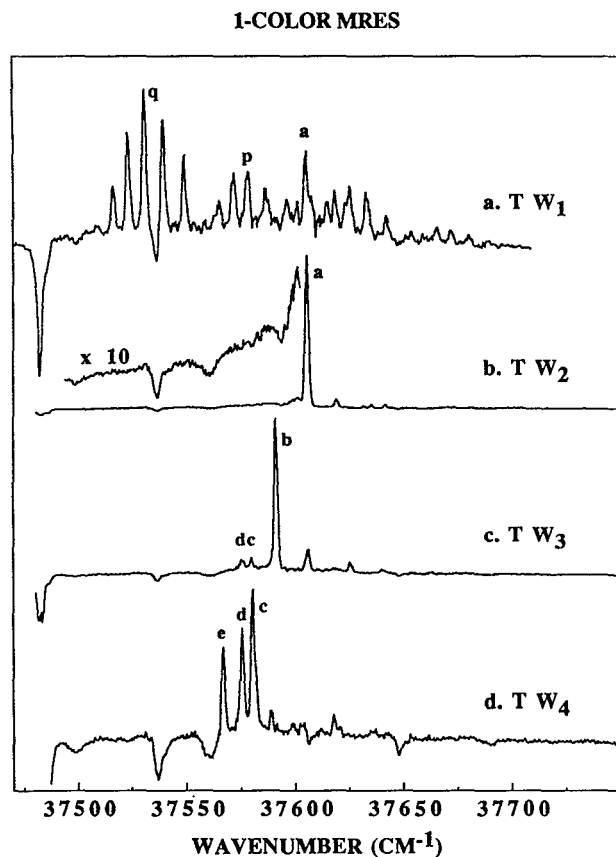


FIG. 1. One-color mass resolved excitation spectra of toluene/water clusters observed in the toluene(H_2O) $_{n-1}$ mass channels. (a) toluene(H_2O), (b) toluene(H_2O) $_2$, (c) toluene(H_2O) $_3$, and (d) toluene(H_2O) $_4$. Features labeled are discussed in the text. The mass channel designations in the figure (TW_m) refer to the detection channels not the true parent cluster masses.

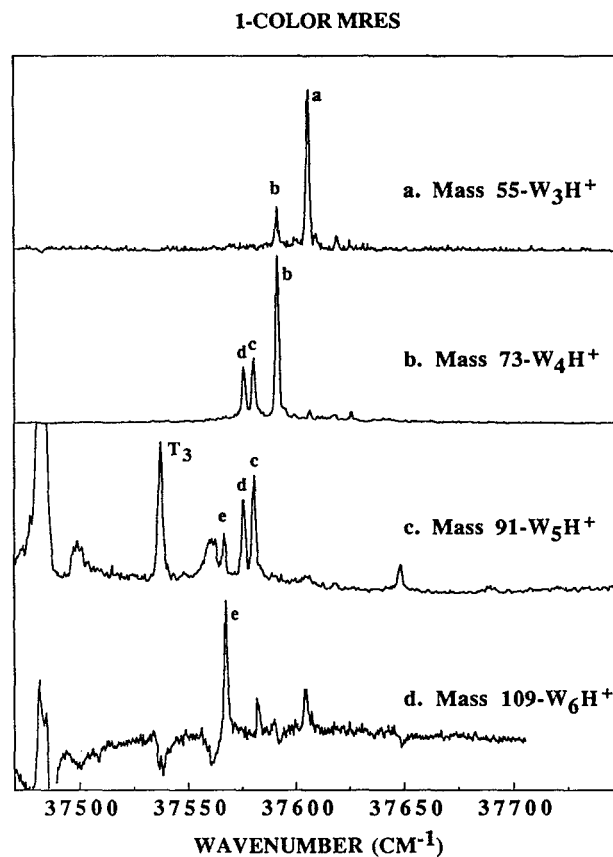


FIG. 2. One-color mass resolved excitation spectra of toluene/water clusters observed in (H_2O) $_n\text{H}^+$ mass channels. (a) (H_2O) $_3\text{H}^+$, (b) (H_2O) $_4\text{H}^+$, (c) (H_2O) $_5\text{H}^+$, and (d) (H_2O) $_6\text{H}^+$. Features are labeled as in Fig. 1.

Peaks labeled **a** and **b** in the toluene(H_2O) $_2$ and toluene(H_2O) $_3$ mass channels are found at 37 606 and 37 591 cm^{-1} , respectively. Features **a** and **b** are followed by weak features at ca. 14 cm^{-1} , to higher energy. Feature **b** is not found in mass channels toluene (H_2O) $_{2,4}$; however, the first small feature following peak **b** in the toluene(H_2O) $_3$ mass channel coincides with peak **a** in the (H_2O) $_{1,2}$ channel. Apparently this feature (**a**) is common to all three mass channels, toluene(H_2O) $_{1,2,3}$: this suggests, in general, that feature **a** in the toluene(H_2O) $_{1,2}$ mass channels may well be a fragment feature associated with toluene(H_2O) $_n$, $n \geq 3$.

Three intense features [**c,d,e**, Fig. 1(d)] are identified in the toluene(H_2O) $_4$ mass channel. Features **d** and **c** also appear in the toluene(H_2O) $_3$ mass channel. The different behavior found for these three features suggests that feature **e** is of different parentage than features **d** and **c**.

One-color MRES also appear for toluene(H_2O) $_n$ clusters in mass channels 55 [$(\text{H}_2\text{O})_3\text{H}^+$], 73 [$(\text{H}_2\text{O})_4\text{H}^+$], 91 [$(\text{H}_2\text{O})_5\text{H}^+$], and 109 [$(\text{H}_2\text{O})_6\text{H}^+$] amu as shown in Fig. 2(a)–2(d). Signals in mass channel 127 [$(\text{H}_2\text{O})_7\text{H}^+$] are too weak to record reliably. One-color MRES for toluene- d_3 (H_2O) $_n$ clusters are also observed in fragment mass channels 56 [$(\text{H}_2\text{O})_4\text{D}^+$], 73 [$(\text{H}_2\text{O})_4\text{H}^+$], and 74

[$(\text{H}_2\text{O})_4\text{D}^+$] as presented in Fig. 3(a)–3(c). All transitions are labeled according to the notation of Fig. 1. Transitions for toluene(H_2O) $_n$ clusters are labeled by unprimed letters (**a,b,c,d,e**) and transitions for toluene- d_3 (H_2O) $_n$ clusters are labeled with primed letters (**a',b',c',d',e'**). The signals observed in mass channel 91 [Fig. 2(c)] are due to both (H_2O) $_5\text{H}^+$ and the benzyl radical ion. Of course, in both instances, the one-color MRES observed is associated with either toluene or the appropriate parent cluster. Features in Fig. 2(c) observed due to the benzyl radical as generated by bare molecule toluene fragmentation are found at 37 482 cm^{-1} (toluene 0_0^0), 37 498, 37 536, and 37 560 cm^{-1} (toluene methyl rotor transitions), and 37 648 cm^{-1} (toluene vibration). The methyl rotor feature at 37 536 cm^{-1} is label T_3 . The transitions **c,d,e**, observed in the 91 amu mass channel [$(\text{H}_2\text{O})_5\text{H}^+$] are the same as observed in the toluene(H_2O) $_4$ mass channel in one-color MRES and thus arise from toluene(H_2O) $_n$, $n \geq 5$ clusters.

The pattern of these results is quite regular: features that appear in the toluene(H_2O) $_{m-1}$ mass channel also appear in the (H_2O) $_m\text{H}^+$ mass channel for $m = 3,4,5$. The following fragment reactions are suggested by the data presented in Figs. 1,2,3:

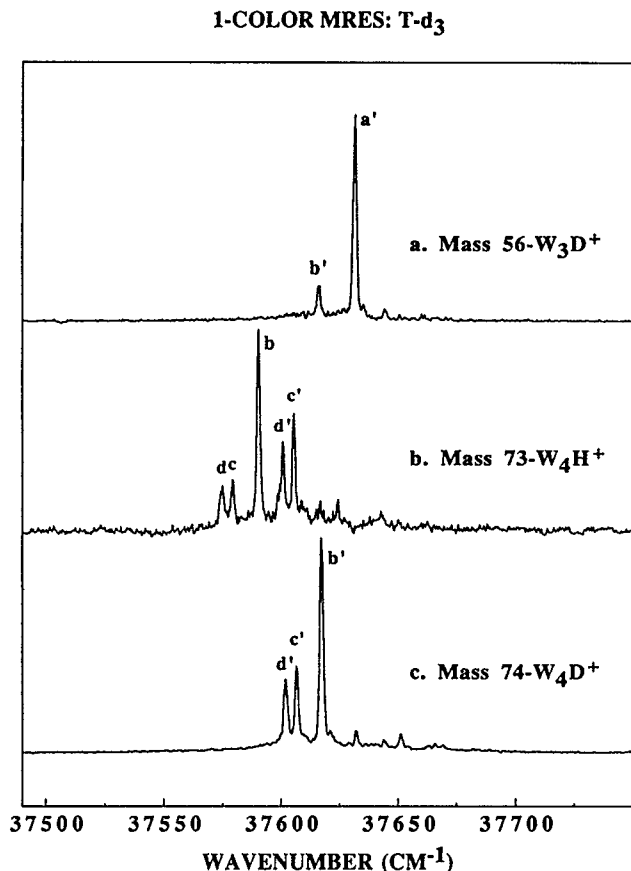
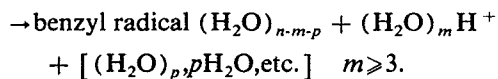
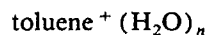
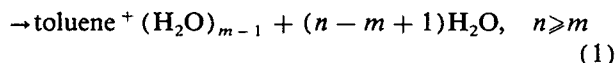
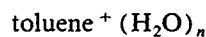
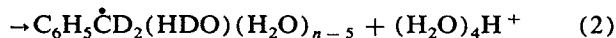
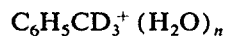


FIG. 3. One-color mass resolved excitation spectra of toluene-d₃/water clusters observed in (H₂O)_xH⁺ (or D⁺) mass channels. (a) (H₂O)₃D⁺, (b) (H₂O)₄H⁺, and (c) (H₂O)₄D⁺. Features are labeled with primed letters to correspond to features found for (H₂O)_x clusters.



One-color MRES signals for toluene-d₃(H₂O)_n can also be found in the (H₂O)₄H⁺ [73 amu, Fig. 3(b)] mass channel. These features are about ten times weaker than those of (H₂O)₄D⁺ [74 amu, Fig. 3(c)]. Features b, c, d are due to residual toluene-h₃/water clusters [compare to Fig. 2(b)]. Features d' and c' (isotopically shifted d and c) are known to be associated with higher order clusters as shown in Fig. 2(c). The MRES spectra presented in Figs. 2(a) (55 amu) and 3(a) (56 amu) and 2(b) (73 amu) and 3(c) (74 amu) are identical except for isotopic shift. One H or D ion must be transferred from the toluene CD₃ or CH₃ methyl group to the (H₂O)_m (m ≥ 3). Thus one can conclude, based on these figures, that the reaction



has taken place. The fact that a b' transition is not found in

the (H₂O)₄H⁺ mass channel [Fig. 3(b)] but is found in the (H₂O)₄D⁺ mass channel [Fig. 3(c)] suggests that H/D exchange as given above is not possible for this transition. This in turn indicates either that the b/b' transition arises from the toluene(H₂O)₄ parent cluster, or that the geometry of this cluster is such that H/D exchange is inhibited. The latter possibility is rather unlikely because the water-water interaction (ca. 2000 cm⁻¹) is much larger than the toluene-water interaction (ca. 600 cm⁻¹).

A general observation about all these fragmentation reaction paths can be made based on the relative intensities of common signals in the different mass channels. Signals observed in the (H₂O)₃H mass channel are several times weaker than the same signals in the toluene(H₂O)₂ mass channel. On the other hand, signals observed in the (H₂O)₅H mass channel are several times stronger than those same signals observed in the toluene(H₂O)₄ mass channel. Thus, fragmentation to toluene(H₂O)₂ is more favorable than fragmentation to the benzyl radical and (H₂O)₃H⁺, but the reaction thermodynamics and/or kinetics change for toluene(H₂O)_n, n ≥ 5. These intensity ratios probably obtain because the proton is better solvated in a (H₂O)₅ cluster than a (H₂O)₃ cluster.

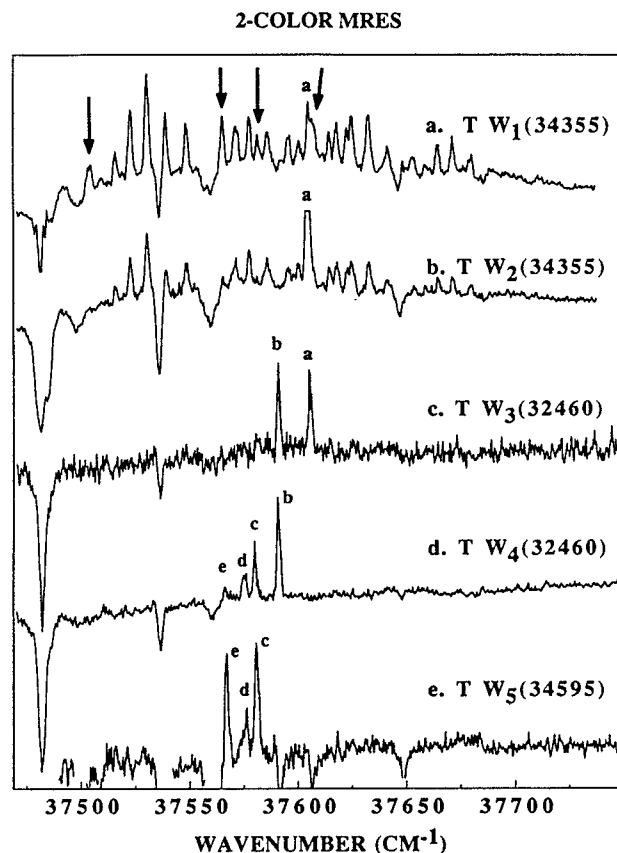


FIG. 4. Two-color mass resolved excitation spectra of toluene/water clusters observed in toluene(H₂O)_x mass channels. Second photon energy is in parentheses. (a) toluene(H₂O)₁, (b) toluene(H₂O)₂, (c) toluene(H₂O)₃, (d) toluene(H₂O)₄, and (e) toluene(H₂O)₅. Features are labeled as in Fig. 1. The arrows in the top spectrum point to new features suggested to be due to toluene(H₂O)₁.

Absence of signals for any feature in the $(\text{H}_2\text{O})_2\text{H}^+$ and $(\text{H}_2\text{O})_1\text{H}^+$ mass channels indicates that cluster fragmentation into these channels is not favorable, most likely due to the relatively low gas phase basicity of $(\text{H}_2\text{O})_{1,2}$: note, however, that the same reaction for toluene/ammonia does generate $(\text{NH}_3)_m\text{H}^+$, $m = 1, 2, 3, \dots$ ⁸

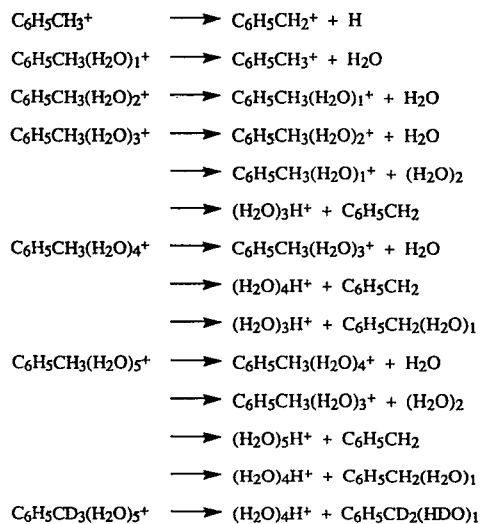
On the basis of the one-color mass resolved excitation thus far presented, multiple cluster conformers for a given cluster mass (size) do not seem to be present.

B. Two-color mass resolved excitation spectroscopy

The two-color MRES observed in toluene $(\text{H}_2\text{O})_n$, $n = 1, \dots, 5$ mass channels are presented in Fig. 4. All one-color toluene $(\text{H}_2\text{O})_{n-1}$ features now clearly appear in the toluene $(\text{H}_2\text{O})_n$ mass channel. Note, in particular, that transition **a** does not appear in the toluene $(\text{H}_2\text{O})_4$ mass channel, and that transition **b** does not appear in the toluene $(\text{H}_2\text{O})_5$ mass channel. Thereby, we suggest that feature **a** is due to toluene $(\text{H}_2\text{O})_3$, feature **b** is due to toluene $(\text{H}_2\text{O})_4$, and feature **c** and **d** are due to toluene $(\text{H}_2\text{O})_5$, etc. Additionally, four new features appear (uniquely) in the toluene $(\text{H}_2\text{O})_1$ mass channel [indicated by arrows in Fig. 4(a)]. We suggest that these four new features actually arise from toluene $(\text{H}_2\text{O})_1$ clusters and that most of the spectra recorded by one-color MRES for this mass channel are due to toluene $(\text{H}_2\text{O})_2$. These conclusions are summarized in Table I and Scheme I.

Scheme I

Observed Fragmentations



To get a clearer picture of the spectrum of the toluene $(\text{H}_2\text{O})_1$ cluster, a difference spectrum between toluene $(\text{H}_2\text{O})_1$ [Fig. 4(a)] and $(\text{H}_2\text{O})_2$ [Fig. 4(b)] is calculated and presented in Fig. 5(a). Transitions marked by the letter O_i ($i = 1, \dots, 4$) are due to toluene $(\text{H}_2\text{O})_1$. Toluene signals appearing in other mass channels are generated by varying degrees of detector overload from the very intense toluene features. The negative peak at $37\,606\text{ cm}^{-1}$ is due to feature **a** [parent toluene $(\text{H}_2\text{O})_3$]. The toluene $(\text{H}_2\text{O})_1$ features can also be observed in the toluene mass channel [Fig.

TABLE I. Identification of labeled transitions (in cm^{-1}).

	Transition energy	Appearance in mass channels	Assignment
t	37 536	1C and 2C toluene	Toluene (internal methyl rotor)
...	37 504	1C toluene; 2CT(W) ₁	T(W) ₁
	37 565		
	37 582		
	37 608		
p	37 579	1C and 2C T(W) ₁ ;	Vibration, T(W) ₂
q	37 531	2C T(W) ₂	
a	37 606	1C and 2C T(W) ₁ , T(W) ₂ , and (W) ₃ H ⁺ ; 2CT(W) ₃	Origin, T(W) ₃
b	37 591	1C and 2C T(W) ₃ , (W) ₃ H ⁺ , and (W) ₄ H ⁺ ; 2C T(W) ₄	Origin, T(W) ₄
c	37 581	1C and 2C T(W) ₃ , T(W) ₄ ,	Origins(?) T(W) ₅
d	37 576	(W) ₄ H ⁺ , and (W) ₅ H ⁺ ; 2CT(W) ₅	
e	37 567	1C and 2C T(W) ₄ , (W) ₅ H ⁺ , and (W) ₆ H ⁺ ; 2C T(W) ₅	Origin, T(W) ₆ or T(W) ₇

2-COLOR MRES: TOLUENE $(\text{H}_2\text{O})_1$

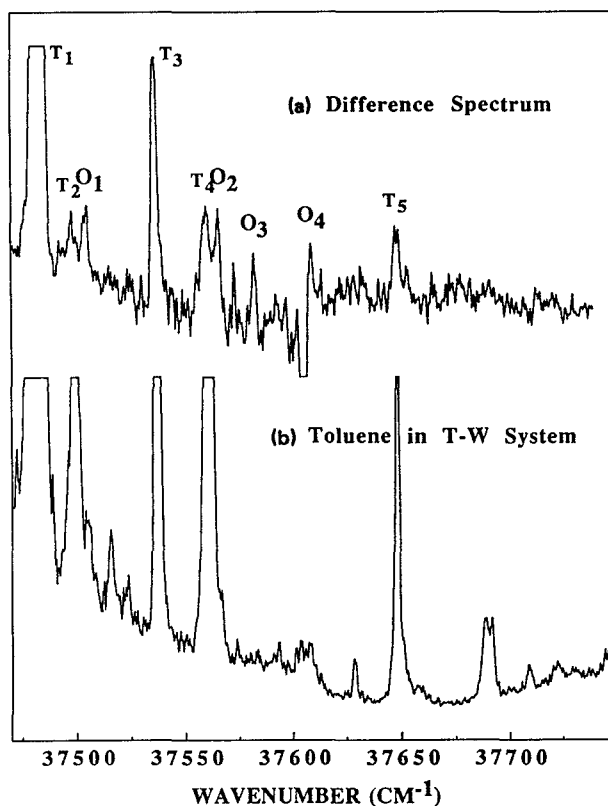


FIG. 5. Identification of parent transitions of toluene $(\text{H}_2\text{O})_1$. (a) The difference spectrum of two-color mass resolved excitation spectra of toluene/water clusters observed in toluene $(\text{H}_2\text{O})_1$ [Fig. 4(a)] and in toluene $(\text{H}_2\text{O})_2$ [Fig. 4(b)] mass channels. T_i are toluene transitions and O_i are toluene $(\text{H}_2\text{O})_1$ transitions. (b) One-color mass resolved excitation spectra of toluene/water clusters observed in the toluene mass channel, in which toluene $(\text{H}_2\text{O})_1$ transitions can be identified.

TOFMS: FEATURE b

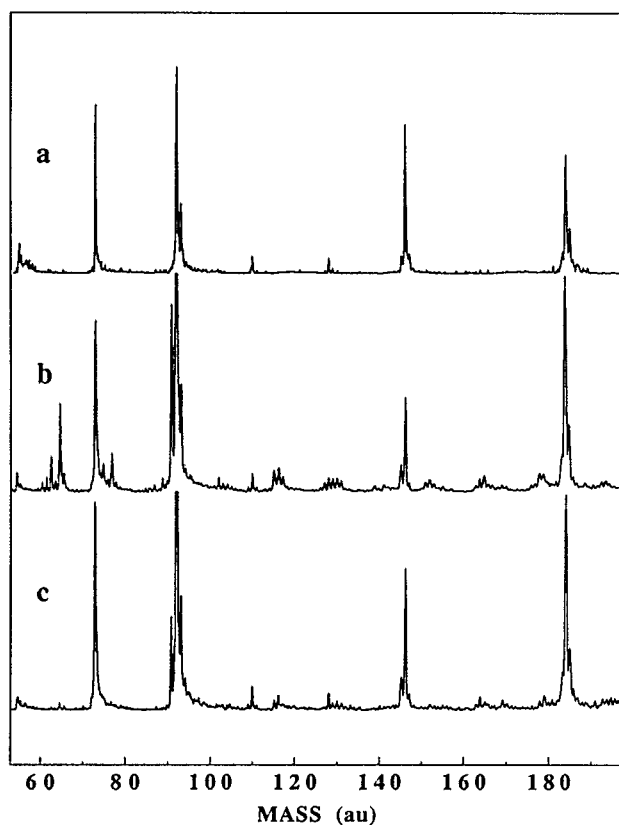


FIG. 6. Time-of-flight mass spectra (TOFMS) of toluene/water clusters. Excitation laser frequency is in resonance with transition b. (a) One-color spectrum, (b) two-color spectrum with ionization laser energy $34\,350\text{ cm}^{-1}$, and (c) the same as (b) but with reduced ionization laser intensity.

5(b)] due to toluene(H_2O)₁ fragmentation.

All observed signals are due to absorption of two and only two photons. This is well illustrated in Fig. 6 in which the transition b (see Figs. 1–4) is excited ($37\,591\text{ cm}^{-1}$) for both one- and two-color mass resolved excitation spectra. The ionization laser is at an energy of $34\,350\text{ cm}^{-1}$ for two-color spectra. If the ionization laser is increased in intensity, new fragments in different mass channels (e.g., 63, 65, 75, 77, 102 amu) can be observed [Fig. 6(b)]. Reducing the laser power slightly returns the mass spectrum to its original low power ionization status [Fig. 6(c)].

C. Time delay studies

In Fig. 7 we present various toluene(H_2O)_n $n = 0, \dots, 6$ signal intensities (labeled as in Figs. 1–4 and Table I) as a function of time delay between nozzle triggering and laser excitation. These data show quite dramatically the following points: (1) the time separation between T_3 and q represents a “double” separation—feature q is due to toluene(H_2O)₂ and T_3 is due to toluene; (2) features p and q are generated by a cluster of the same mass, toluene(H_2O)₂; (3) heavier mass clusters are formed more closely together in the expansion and suffer flight time and/or condensation compression as can be seen from the time delay behavior of features q, a, b, c. These data firmly establish the following: (1) feature e is

RELATIVE NOZZLE/LASER DELAY

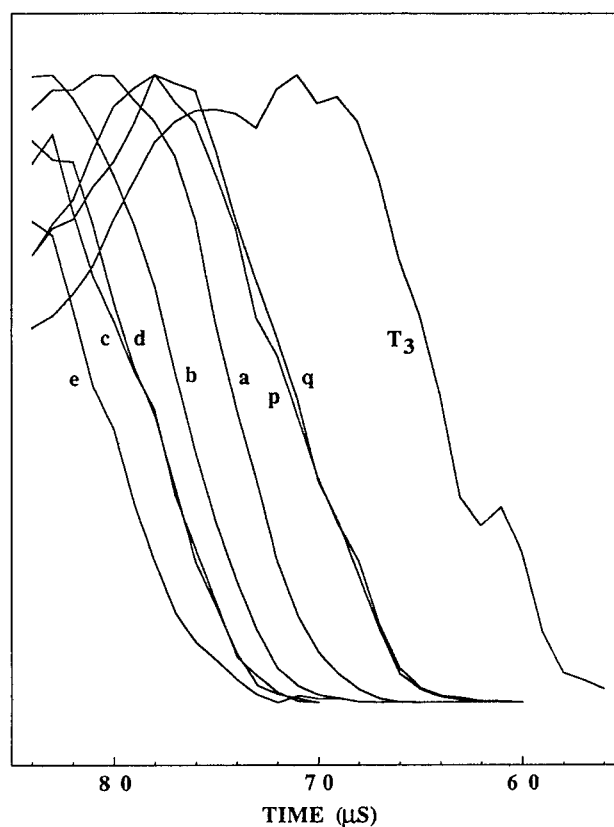
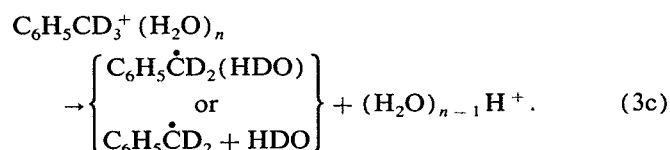
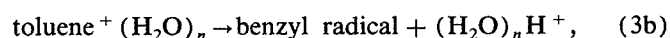
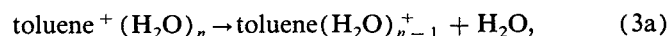


FIG. 7. Pulsed-nozzle/excitation-laser timing effect on signal intensities. These data can be used to associate specific cluster masses with specific transitions. See text for discussion.

generated by parent toluene(H_2O)₆ or (H_2O)₇; (2) features c and d are generated by parent toluene(H_2O)₅; (3) feature b is generated by toluene(H_2O)₄; (4) feature a is generated by toluene(H_2O)₃; (5) features p and q are generated by toluene(H_2O)₂; and (6) the missing toluene(H_2O)₁ cluster spectra are located by two-color MRES techniques and are presented in Fig. 5 as O_1 . These conclusions are summarized in Table I and Scheme I.

Some additional general comments can now be made regarding the fragmentation processes observed: (1) the typical fragmentation reactions presented in Eq. (1) hold mainly with $m = n$ and $p = 0$; (2) the benzyl radical is generated usually without solvation; and (3) toluene/water cluster geometry is such that H/D exchange [as depicted in Eq. (2)] can occur for the larger toluene- d_3 /water clusters. These results are summarized in the following equations:



Two-color MRES studies as a function of time delay between the two lasers have been performed for all the la-

beled transitions **a,b,c,d,e**. For example, transition **a** signals observed in all three mass channels, $(\text{H}_2\text{O})_3\text{H}$, toluene $(\text{H}_2\text{O})_2$, and toluene $(\text{H}_2\text{O})_3$, have identical lifetimes of about 65 ns: this is the same lifetime as the toluene S_1 state. We thus conclude that the observed chemistry and energy dynamics of the toluene/water system are not related in any way to the toluene triplet manifold or the ground state: all the competitive fragmentation reactions that are observed for the toluene/water system must take place in the ground electronic state of the ion. Recall that all presented excitations $S_1 \leftarrow S_0$ take place with no vibrational excess energy generated in the cluster.

The third time dependent measurement needed to help elucidate the mechanisms and kinetics of the observed dissociation and proton transfer/fragmentation reactions is a study of the signal intensity as a function of flight time: in particular we are concerned about signal "line shape" for given mass channel features. These one-color and two-color MRES results are displayed in Fig. 8. The transitions presented are feature **a** detected in the $(\text{H}_2\text{O})_3\text{H}$ mass channel, feature **T**₃ detected in the toluene mass channel, and feature **a** detected in both the toluene $(\text{H}_2\text{O})_2$ fragment and toluene $(\text{H}_2\text{O})_3$ parent mass channels (see Figs. 1-4 and Table I). Transition **a** in the $(\text{H}_2\text{O})_3\text{H}$ mass channel [Fig. 8(a)] rises in mass channel 55 amu, but spreads (decays) to "higher mass channels" or longer flight times. In the two-color experiment the ionization laser energy is varied between 34 636 and 37 600 cm^{-1} with no effect on the observed signal time width. On the other hand, transition **a** detected in the toluene $(\text{H}_2\text{O})_2$ mass channel does not show this "decay behavior" [Fig. 8(c)]. Moreover, neither do any of the other signals [Figs. 8(b) and 8(d)].

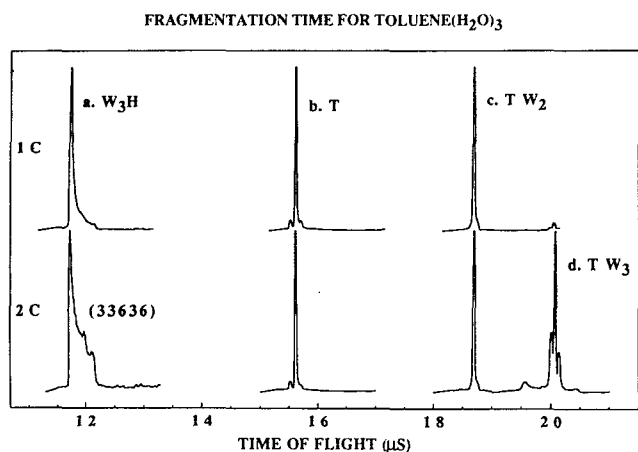
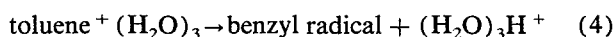


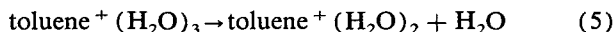
FIG. 8. One-color (top) and two-color (bottom) time-of-flight mass spectra of toluene/water clusters. Except for the toluene bare molecule signal, excitation laser frequency is in resonance with transition **a**. (a) cluster signal observed beginning with $(\text{H}_2\text{O})_3\text{H}^+$ mass channel, (b) toluene signal observed in toluene mass channel, (c) cluster signal observed in toluene $(\text{H}_2\text{O})_2$ mass channel, and (d) cluster signal observed in parent toluene $(\text{H}_2\text{O})_3$ mass channel. Identical behavior is observed for the $(\text{H}_2\text{O})_3\text{D}$ and toluene- $\text{d}_3(\text{H}_2\text{O})_2$ mass channels with the toluene- $\text{d}_3(\text{H}_2\text{O})_3$ parent cluster feature **a'** accessed. Extra features observed in the two-color mass spectrum of $(\text{H}_2\text{O})_3\text{H}^+$ are due to fragmentation caused by multiphoton ion absorption. While only the one-color feature is analyzed in detail, both are found to have the identical decay time constants.

We note the following additional information concerning these observations: (1) exactly the same behavior is found for transition **a'** of the toluene- $\text{d}_3(\text{H}_2\text{O})_3$ as detected in the $(\text{H}_2\text{O})_3\text{D}$ (56 amu) mass channel; (2) the width of the mass channel 55 and 56 amu features is due to a single mass peak and a single, resolved spectroscopic feature (**a** and **a'** in this instance); (3) various positions in the width of roughly eight to ten mass channels yield the same optical spectrum (feature **a** or **a'**); (4) the apparent sharp features to higher mass in the two-color signal at mass channel 55 amu are due to fragmentation associated with the high intensity of the ionization laser needed to generate the intense feature displayed; and (5) both the one-color and two-color MRES signals in mass channel 55 and 56 amu give the same decay constants.

These observations suggest that the reaction



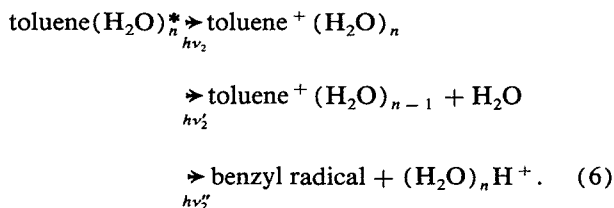
takes place slowly (ca. 500 ns). Upon careful analysis of the line shape of the 55 amu $(\text{H}_2\text{O})_3\text{H}^+$ time of flight signal, this feature can be resolved into a < 60 ns and a 480 ns generation time, as will be shown below. On the other hand, the reaction



can be deconvolved into only a ca. < 60 ns generation time [the instrument response function in roughly 20 ns full width at half maximum (fwhm)] after the parent cluster has been ionized. These data suggest the following physical behavior for the fragmentation of the toluene $(\text{H}_2\text{O})_3$ cluster: (1) two pathways exist to generate the $(\text{H}_2\text{O})_3\text{H}^+$ fragment, one fast < 60 ns and one slow ca. 480 ns; and (2) a single pathway exists to generate the toluene + $(\text{H}_2\text{O})_2$ fragment. Contributions from fragmentation kinetic energy render a better estimate of the fast generation time difficult to make. A detailed discussion of the analysis of these MRES line shapes is presented in the Discussion section.

D. Apparent threshold ionization energies

Ionization action spectra are recorded for each cluster as detected through the parent and fragment mass channel signals. Thus, an appearance or apparent ionization energy can be found for each reaction



The * indicates the cluster is in its S_1 excited state. A few examples of such spectra are presented in Fig. 9. Figure 9(a) shows the ionization action spectrum of transition **T**₃ of bare toluene. The toluene transitions have a sharp ionization threshold with a $\Delta v = 0$ Franck-Condon factor maximum. Clusters with nonpolar solvents typically have similar ionization threshold behavior as shown for benzene $(\text{CH}_4)_1$ in Fig. 9(b). On the other hand, toluene $(\text{H}_2\text{O})_2$ has a gradual-

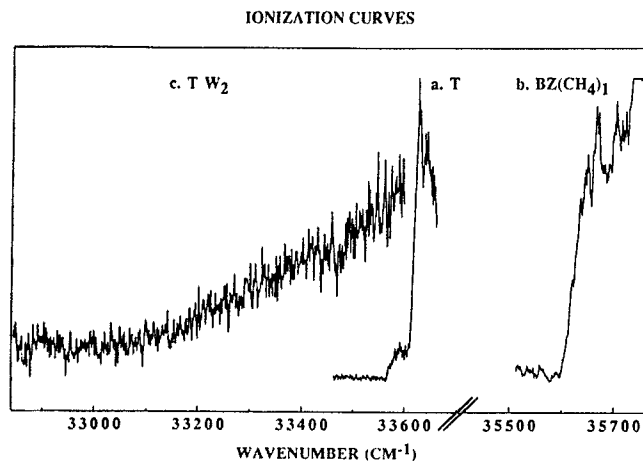


FIG. 9. Ionization action curves. (a) toluene, (b) benzene(methane)₁, and (c) toluene(H₂O)₂.

ly increasing threshold over several thousands of cm⁻¹. Figure 9(c) shows the first ~500 cm⁻¹ of this slow rise for the transition labeled *q* in Figs. 1–4 and Table I. For this latter cluster the Franck–Condon factor must favor large $\Delta\nu$ and therefore the two accessed potential surfaces *S*₁ and *I* must be displaced from one another and of a different shape. The behavior displayed for toluene(H₂O)₂ transition *q* in Fig. 9(c) is typical of all toluene/water cluster transitions. The *S*₁ and *I* states must have significantly different geometries for the toluene/water cluster system.

Threshold ionization data for the various parent clusters detected in the toluene(H₂O)_{*n*}, toluene(H₂O)_{*n*-1}, and (H₂O)_{*n*}H mass channels are presented in Table II. The parent cluster will generate three different products depending on the ionization energy. For example, the toluene⁺(H₂O)₄ appears at a threshold energy of 68 940 cm⁻¹. The toluene⁺(H₂O)₃ product requires 1300 cm⁻¹ more energy to appear and the (H₂O)₄H⁺ fragment requires 1100 cm⁻¹ more energy to appear. These data are summarized in Table II.

From the data presented in Table II one can extract the following generalizations concerning toluene/water ioniza-

TABLE II. Apparent ionization energy of toluene(H₂O)_{*n*} [T(H₂O)_{*n*}] in cm⁻¹ as detected by the appearance of different observed fragment signals. The numbers in parentheses are the excess energies associated with the one-color ionization for each parent species and fragment.

Parent cluster	T (<i>n</i> = 0)	T(H ₂ O) ₁ (<i>n</i> = 1)	T(H ₂ O) ₂ (<i>n</i> = 2)	T(H ₂ O) ₃ (<i>n</i> = 3)	T(H ₂ O) ₄ (<i>n</i> = 4)
Observed in mass channel					
T(H ₂ O) _{<i>n</i>}	71 090 (3 870)	71 070 (3 950)	70 640 (4 420)	70 075 (5 140)	68 940 (6 240)
T(H ₂ O) _{<i>n</i>-1}			71 660 (3 400)	71 855 (3 360)	70 270 (4 910)
(H ₂ O) _{<i>n</i>} H ⁺				(70 940) (4 280)	(70 060) (5 120)

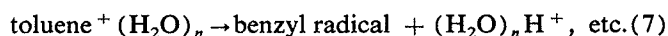
tion thresholds for reaction: (1) the ion state in the toluene/water cluster system is significantly stabilized with respect to the *S*₀ and *S*₁ cluster state and the bare toluene molecule, especially for large clusters; (2) the appearance potential for the (H₂O)_{*n*}H⁺ product is lower than that for the toluene⁺(H₂O)_{*n*-1} product for *n* ≥ 3; and (3) fragmentation of higher order clusters [see Eq. (3)] into the toluene(H₂O)_{1,2} channels takes more energy than fragmentation into the toluene(H₂O)₃ mass channel.

IV. DISCUSSION

Two different types of fragmentation are observed



and



Cluster ion fragmentation to (H₂O)_{*m*}H⁺ is possible as long as *m* ≥ 3. This behavior is probably related to the gas phase basicity of water because toluene/ammonia cluster can fragment to (NH₃)_{*y*}H⁺, *y* = 1,2,3,...

These two paths as governed by intracluster vibrational redistribution (IVR), vibrational predissociation (VP), proton transfer, and overall reaction energy balance. The simple dissociation reactions must be governed by IVR and VP kinetics. The proton transfer/dissociation reaction is governed by the stability of the products which include the benzyl radical, and the solvated proton. Evidently the proton affinities (properly, gas phase basicities) of H₂O and (H₂O)₂ are not large enough to drive the reaction for H₃O⁺ and (H₂O)₂H⁺. Since both the binding energies and the Franck–Condon shift for the *I* ← *S*₁ transition are unknowns, we cannot be more specific concerning the energy balance and dynamics of these two paths.

A. Cluster structure

While only limited information concerning cluster geometry is available from the data presented in this report, some qualitative notions of cluster structure can be gained from these results.

First, we suggest that the water molecules in these clusters are themselves clustered into *n*-mers for the following reasons: spectroscopic shifts are all small and similar for the *S*₁ ← *S*₀ transition in the various toluene(H₂O)_{*n*} clusters; the parent clusters readily fragment into large (H₂O)_{*n*}H⁺ (*n* = 3,4,5,6) clusters; and each toluene(H₂O)_{*n*} (*n* = 2,3,4,6...) cluster has a spectrum comprised typically of a single origin feature. The latter point suggests the water cluster forms in the presence of toluene and then interacts with it, consistent with the relative size of the (H₂O)_{*n*} interaction energy (ca. 2000 cm⁻¹/H₂O) and the toluene/water interaction energy (ca. 600 cm⁻¹/H₂O).

Second, an inner (*n* < 3) and outer (*n* > 3) layer of water molecules seems to be consistent with the experimental results. The data that suggest this type of structure are the following: toluene(H₂O)_{*n*} (*n* = 2,3, and 4) fragmentation appearance energy differs for the toluene(H₂O)_{*n*-1} cluster mass channel (see Table II); similarity between toluene(H₂O)₃ and toluene(H₂O)₄ spectra (features *a* and *b*,

in Figs. 1–4 and Table I) suggests the fourth H_2O does not interact strongly with toluene; cluster geometry seems to change significantly upon excitation for toluene(H_2O) $_n$ ($n < 2$) but not larger ($n > 3$) clusters; cluster $S_1 \leftarrow S_0$ energy shifts are greatest for $n < 3$ but almost nonexistent for $n > 4$; and higher order clusters [toluene(H_2O) $_{3+m}$ for $m > 0$] fragment into the toluene(H_2O) $_3$ mass channel but not into the toluene(H_2O) $_{1,2}$ mass channels [consider the behavior of feature **a** vs feature **b** (see Figs. 1–4 and Table I)].

Third, the water molecules probably hydrogen bond together in a chain or cyclic structure because of the limited number of cluster configurations for a given parent cluster $n = 1, \dots, 4$.

Empirical potential energy calculations can be employed to obtain additional insight into the details of cluster structure for small toluene/water clusters ($n = 1, 2$). All calculations for the S_0 state of toluene(H_2O) $_1$ suggest that the hydrogen atoms of water point toward the aromatic ring, in a “weak hydrogen bonding” interaction geometry. The S_1 cluster structure should be fairly similar, even though the $n = 2$ toluene/water cluster does undergo some water displacement upon excitation. This would clearly not be the best structure for the toluene(H_2O) $_n$ cluster ions because the positive ring would be best solvated by the negative end of the water dipole pointed toward it. We thus expect a large geometry change upon $I \leftarrow S_1$ excitation for these clusters: a rotation of the water molecule(s) in the toluene/water cluster, such that in the cluster ion state the oxygen atom of water would be closest to the ring, would be consistent with this picture.

B. Fragmentation patterns and mechanisms

Parent clusters, their transitions and fragmentation paths are presented in Table I. A general summary of the fragmentation patterns observed is presented in Scheme I. Note that for all toluene/water clusters, fragmentation is nearly complete: even near threshold ionization, ion fragmentation is a dominant factor in the cluster ion behavior and detection. Similar and even more extensive fragmentation is also found for the toluene/ammonia cluster system.

Such extensive fragmentation is not usual for van der Waals clusters. For example, even one-color MRES spectra of simple aromatics (e.g., benzene, toluene, azines, etc.) clustered with nonpolar solvents^{1,10} (e.g., rare gases but not He, $\text{C}_n\text{H}_{2n+2}$, CF_4 , CO_2 , CO , N_2) do not show extensive fragmentation reactions. One would initially suggest that, since the binding energies in S_0 , S_1 , and I for polar solvents should be much larger than those for nonpolar solvents, cluster ion fragmentation should be even less of a problem for aromatic/polar solvent clusters than it is for aromatic/nonpolar solvent clusters. Nonetheless, this is clearly not the case and we can present two related arguments to make the observed extensive cluster ion chemistry seem reasonable. First, the cluster ion is much more tightly bound than either the S_0 or S_1 van der Waals toluene(H_2O) $_n$ cluster in its equilibrium configuration. Therefore, not only is the ion cluster potential well deeper, but its equilibrium minimum is also shifted to smaller separation between aromatic and solvent. Additionally, as pointed out above, the water molecule ori-

entation for the closest waters to the toluene ring should have a different (probably inverted) equilibrium ring orientation in the ion than they do in the S_0 or S_1 states. This equilibrium position shift ensures (through the Franck–Condon factor for the transition $I \leftarrow S_1$) that the optically accessed ion is highly vibrationally excited and $\Delta v \gg 0$ for the $I \leftarrow S_1$ transition. The cluster ion then even at “threshold ionization” can have a great deal of excess vibrational energy. This too explains the very broad threshold for the ion excitation spectra: the slope in Fig. 9(c) represents the vibrational overlap for the Franck–Condon transition $I \leftarrow S_1$. This slope probably reflects the ion potential surface curve many thousands of wave numbers above the ion zero point state. Second, if the polar solvent can accept a proton [e.g., $(\text{H}_2\text{O})_n\text{H}^+ n \geq 3$ and $(\text{NH}_3)_m\text{H}^+$, $m \geq 1$] and thereby generate a very stable radical (e.g., benzyl), the overall fragmentation reaction becomes much more energetically favorable.

C. Fragmentation kinetics

One additional piece of information is available concerning the fragmentation reactions. For toluene $^+(\text{H}_2\text{O})_3$, the fragments toluene $^+(\text{H}_2\text{O})_{1,2}$ and $(\text{H}_2\text{O})_3\text{H}^+$ are observed. The dissociation reaction is relatively fast (< 60 ns) and proton transfer fragmentation [i.e., $(\text{H}_2\text{O})_3\text{H}^+$ generation] has both slow ($\tau_2 \sim 500$ ns) and fast ($\tau_1 < 60$ ns) components (see Fig. 8).

To obtain the above information from the width of these observed fragment mass channel signals, we must relate the observed (detector) time to real time in the molecular frame. A number of points must be considered in this regard: (1) the time-of-flight mass spectra (TOFMS) signal is a function of time T as detected by the microchannel plate mass detector; (2) T is an implicit function of the fragmentation (real) time (t) of the parent clusters; (3) all signals are convolved with the instrument response function, as given by the toluene bare molecule signal; and (4) the mapping between t and T is a function of instrument parameters and the respective masses of the parent and fragment clusters, and thus different signal widths for different fragments arising from a given parent do not necessarily imply different kinetics for each fragment.

To determine the lifetime of the immediate precursor of $(\text{H}_2\text{O})_3\text{H}^+$ and to determine whether or not the fragments $(\text{H}_2\text{O})_3\text{H}^+$ and toluene $^+(\text{H}_2\text{O})_2$ have a common precursor before their formation, the time mapping for different ions ($t \leftrightarrow T$) must be found. This mapping is accomplished under the following assumptions: (1) the ion is formed at time zero at a single point within the ion extraction region; (2) parent clusters and their fragments have no initial velocity along the direction of the flight tube; and (3) the ions are only directed by the applied electric field, not the presence of other ions. The resulting formulas are listed in Table III. Also presented is a flight time calculation for fragmentation occurring in the acceleration region. Evidently several factors which may potentially contribute to the observed signal (flight time) width have been ignored by these assumptions. The most significant one is probably the kinetic energy release associated with the various fragmentation channels. This initial fragment kinetic energy contribution to the ion

TABLE III. Time mapping between T as detected by the microchannel plate (MCP) detector and the real fragment time t after ionization.

Fragmentation in the extraction region (3.988–3.655 kV).

$$T = \sqrt{\frac{2}{e}} \left\{ \left(\frac{S_f M_p}{E_1} \right)^{1/2} + \sqrt{M_f} \left[\left(\frac{S_f C + S_1}{E_1} \right)^{1/2} - \left(\frac{S_f M_f}{E_1 M_p} \right)^{1/2} \right. \right. \\ \left. \left. + \left(\frac{E_1}{E_2^2} (S_f C + S_1) + \frac{S_2}{E_2} \right)^{1/2} - \left(\frac{E_1 (S_f C + S_1)}{E_2^2} \right)^{1/2} \right. \right. \\ \left. \left. + \frac{S_3}{2} (E_1 (S_f C + S_1) + E_2 S_2)^{-1/2} \right] \right\} \\ t = \left(\frac{2 S_f M_p}{E_1 e} \right)^{1/2}$$

Fragmentation in the acceleration region (3.655–0.0 kV)

$$T = \sqrt{\frac{2}{e}} \left\{ \sqrt{M_p} \left[\left(\frac{S_1}{E_1} \right)^{1/2} + \left(\frac{S_1 E_1}{E_2^2} + \frac{S_f - S_1}{E_2} \right)^{1/2} - \left(\frac{S_1 E_1}{E_2^2} \right)^{1/2} \right. \right. \\ \left. \left. + \sqrt{M_f} \left[\left(\frac{S_1 E_1 M_f}{E_2^2 M_p} + \frac{C(S_f - S_1)}{E_2} + S_2 \right)^{1/2} \right. \right. \right. \\ \left. \left. - \left(\frac{M_1}{E_2 M_p} \left(\frac{S_1 E_1}{E_2} + S_f - S_1 \right) \right)^{1/2} \right. \right. \right. \\ \left. \left. + \frac{S_3}{2} \left(\frac{S_1 E_1 M_f}{M_p} + S_2 E_2 + C E_2 (S_f - S_1) \right)^{-1/2} \right] \right\} \\ t = \sqrt{\frac{2 M_p}{e}} \left[\left(\frac{S_1}{E_1} \right)^{1/2} + \left(\frac{S_1 E_1}{E_2^2} + \frac{S_f - S_1}{E_2} \right)^{1/2} - \left(\frac{S_1 E_1}{E_2^2} \right)^{1/2} \right]$$

The first derivative evaluated at $t = 0$

$$\left. \frac{dT}{dt} \right|_{t=0} = -C$$

Definition of symbols used.

T = total flight time or the detected time.

t = fragmentation time.

S_0 = 12 mm, distance between the bottom and the middle grids (3.988–3.655 kV).

S_1 = 7 mm, distance between the ionization position and the middle grid.

S_f = distance between the ionization and the fragmentation positions.

S_2 = 12 mm, distance between the middle and the top grids.

S_3 = 1480 mm, distance between the top grid and the MCP detector.

M_p = 146 amu, parent ion mass.

M_f = 55 or 128 amu, fragment ion mass.

E_1 = (3988–3655 V)/ S_0 , electric field in the extraction region.

E_2 = 3655 V/ S_2 , electric field in the acceleration region.

$C = M_f/M_p - 1$.

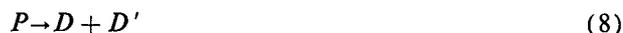
flight time and its spread will be estimated in the ensuing discussion. All other contributions to the flight distribution for a given ion should effect all ions equally and thus may be included in the instrument response function (i.e., the observed width of the toluene⁺ signal).

Employing these two expressions with the experimental parameters given in Table III, one readily determines that the observed signal is generated only by cluster parent ion fragmentation in the ion extraction region. Since the electric field is so large in the acceleration region and the clusters spend so little time in this portion of the mass spectrometer, fragmentation in this region only contributes to the broad (unobserved) background signal extending from the frag-

ment mass channel to the parent cluster [toluene(H_2O)₃] mass channel. Therefore, the observed signal width for (H_2O)₃H⁺ in either one- or two-color TOFMS (ca. 500 ns) is not directly related to any lifetime: this width merely indicates that the lifetime of the precursor of (H_2O)₃H⁺ is long enough that this cluster reaches the ion extraction grid with sufficient concentration for (H_2O)₃H⁺ to be detected following its fragmentation.

In fitting the signals for (H_2O)₃H⁺ and toluene⁺(H_2O)₂ fragments of the parent toluene(H_2O)₃ clusters three constraints must be considered. First, the detected signal is proportional to $d[D]/dT$ (T = detector time) and not the daughter fragment concentration $[D]$. Second, ¹³C-toluene contributes equally to the toluene(H_2O)_{2,3} signals but not to the (H_2O)₃H⁺ signal. Third, the observed “two-color” signal intensities of (H_2O)₃H⁺ and toluene⁺(H_2O)₂ have different actual one-color and two-color signal contributions and therefore only the one-color MRES data are chosen for fitting and analysis.

Consider the general reaction



in which P is the immediate precursor of the daughter fragments D, D' . Then

$$\frac{d[D]}{dt} = k[P] \quad (9)$$

and the fragment signal intensity as a function of time t would exponentially decay as the total concentration of P decays. (In the ensuing discussion we simplify the notion $[D]$ and $[P]$ to D and P , respectively.) The fitting process thus involves the following steps: (1) assume an exponential decay for P as a function of t , $P = P[t]$; (2) $dD/dt = k[P(t)]$; (3) find dD/dT by converting detector time T into real time t , such that

$$\frac{dD}{dT} = \left(\frac{dD}{dt} \right) \left(\frac{dt}{dT} \right) = k [P\{t(T)\}] \left(\frac{dt}{dT} \right); \quad (10)$$

and (4) convolve dD/dT represented in T with the appropriate instrument response function.

From the formulas given in Table III, one can readily determine that both $t(T)$ and dt/dT are required for the fitting and analysis procedure. A similar formula has been given for fragmentation in the ion extraction region only¹¹ (note some corrections, however), but dt/dT has not been employed. This derivative can be calculated from the expression for T given in Table III or can be approximated from $\Delta t/\Delta T$ away from the initial $t = 0$ point. Since the signal height is only known in a relative measure and is adjusted for a given scan, the reaction constant k in Eq. (10) does not directly enter into the analysis except as a scale factor.

Employing the equations given above and in Table III, the curve for the (H_2O)₃H⁺ signal can only be fit with two exponentials. The generation times are $\tau_1 = 60$ ns and $\tau_2 = 480$ ns: these decay times refer to the precursor decay times and suggest that the (H_2O)₃H⁺ ion is generated by two different pathways. This fit is shown in Fig. 10(a) in which the dashed curve is the experimental result and the solid curve is the biexponential fit with τ_1 and τ_2 . The same two lifetimes for the precursor give a poor fit to the experi-

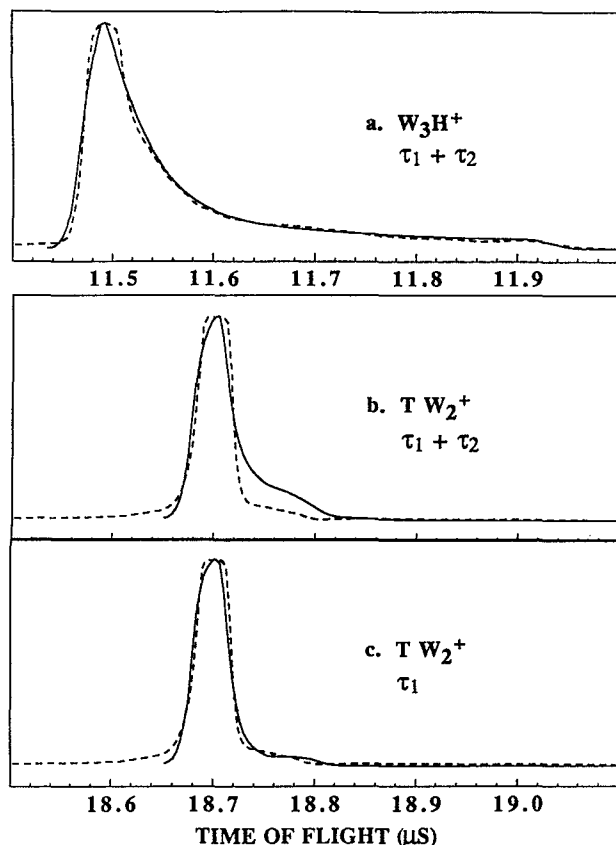


FIG. 10. Expanded one-color time-of-flight mass spectra of toluene/water clusters, in resonance with transition **a**. Dashed line is the experimental data in Fig. 8(a)–8(c) and the solid line is the calculated fit. (a) Cluster signal observed beginning with the $(\text{H}_2\text{O})_3\text{H}^+$ mass channel and fit to 480 and 60 ns generation times, (b) cluster signal observed in toluene $(\text{H}_2\text{O})_2$ mass channel and fit to the same weight of 480 and 60 ns generation times, and (c) cluster signal observed in the toluene $(\text{H}_2\text{O})_2$ mass channel and fit with 60 ns generation time only.

mental signal for toluene $(\text{H}_2\text{O})_2$ as displayed in Fig. 10(b): clearly the long lifetime ($\tau_2 \sim 480$ ns) is not appropriate for this signal. If only a single exponential with $\tau_1 = 60$ ns is fit to the experimental curve as shown in Fig. 10(c), a good reproduction of the experimental signal for the toluene $(\text{H}_2\text{O})_2$ fragment cluster obtains.

One can readily estimate the flight time spread due to initial kinetic energy of the fragment. Assuming a fragment mass of 100 amu and an initial kinetic energy of the fragment of 14 kcal/mol (~ 4900 cm^{-1}), the ion speed is 4.62×10^6 cm/s. A fragment ion of this speed moving away from the flight tube and mass detector would return to its original (creation) position in ~ 16 ns: this time is close to the instrument response function of 20 ns FWHM. The time of flight signal for toluene $^+(\text{H}_2\text{O})_2$ (see Fig. 8) is only somewhat wider than that of toluene. Thus the short lifetime τ_1 is stated as a maximum value: the actual generation time may be considerably less than the stated $\tau_1 < 60$ ns. The exact value of this fast component, however, does not affect any of the ensuing discussion of the cluster fragmentation kinetics and possible mechanisms.

One can model these kinetic data with a number of dif-

ferent possible mechanistic schemes but they must all have the following similarities: (1) the $(\text{H}_2\text{O})_3\text{H}^+$ fragment is generated from two different precursors; (2) these precursors must have the same charge and the mass as the precursor for the toluene $^+(\text{H}_2\text{O})_2$ fragment; (3) the precursor with the long lifetime ($\tau_2 \sim 480$ ns) cannot be the nascent state toluene $^+(\text{H}_2\text{O})_3$ and is probably generated by either IVR or proton transfer; and (4) the precursor of toluene $^+(\text{H}_2\text{O})_2$ and the long lifetime precursor of $(\text{H}_2\text{O})_3\text{H}^+$ must not be the same.

Without further detailed information concerning the structure, binding energy, and vibrational levels of the toluene $^+(\text{H}_2\text{O})_{2,3}$ and $(\text{H}_2\text{O})_3\text{H}^+$ clusters, we cannot analyze the cluster ion reaction dynamics further. We note, however, that a simple (classical) Rice–Ramsperger–Kassel–Marcus (RRKM) calculation of the form

$$k \propto c \left(\frac{E - E_0}{E} \right)^{S-1} h\nu,$$

with E = total energy of cluster, E_0 = binding energy of the cluster, $c = 3 \times 10^{10}$ cm/s, $h\nu = 100$ cm^{-1} , $S = 18$, and $(E - E_0)/E \sim 0.75$ to 0.45 yields $\tau \sim 40$ ps to 300 ns. This range is reasonable in both time and energy balance for the overall reaction [Eq. (7)] dynamics observed.

In larger clusters [toluene $^+(\text{H}_2\text{O})_{3+m}$, $m = 1, 2, 3, \dots$] the energy balance is probably such that the proton transferred clusters containing the benzyl radical fragment much more rapidly. Only for the toluene $(\text{H}_2\text{O})_3$ cluster is the gas phase basicity, benzyl radical solvation energy, and benzyl radical/ $(\text{H}_2\text{O})_3\text{H}^+$ binding energy such that the reaction kinetics can be resolved with a ~ 20 ns FWHM instrumental response function.

These dynamics (i.e., fragment cluster generation times) are not observed for larger clusters such as toluene $^+(\text{H}_2\text{O})_{4,5,6}$ for which enhanced cluster ion binding energies and enhanced basicities of the large water clusters yield a more highly vibrationally excited nascent state.

V. CONCLUSIONS

These studies of the ion chemistry in the toluene/water system have generated a number of conclusions. A summary of the reactions found, spectra assigned, and energy thresholds for the different dynamical behavior observed can be found in Tables I and II and Scheme I.

The general conclusions of this work can be stated as follows:

(1) Toluene/water cluster ions undergo extensive fragmentation following one- or two-color ($I \leftarrow S_1 \leftarrow S_0$) ionization. The favored fragmentation pathway for toluene $(\text{H}_2\text{O})_n$, $n \leq 4$, is loss of a water molecule. At one-color excess energies (Table II), generation of toluene $(\text{H}_2\text{O})_{n-1}$ by loss of a water molecule accounts for over 50% of the signal. The favored fragmentation pathway for toluene $(\text{H}_2\text{O})_n$, $n \geq 5$ is the generation of $(\text{H}_2\text{O})_n\text{H}^+$.

(2) The number of toluene/water cluster geometries is quite small. Most clusters display a single spectroscopic origin and thus a single conformation for $n = 1, \dots, 6$. The water molecules also seem to aggregate together (hydrogen bond) on one side of the toluene ring. Cluster structure is suggested

to be arranged in solvent shells with three water molecules forming a first shell and the others lying in a second shell.

(3) Toluene⁺(H₂O)_n cluster ions ($n \geq 3$) can generate a benzyl radical and H⁺(H₂O)_{3+m} ($m = 0, 1, 2, \dots, n-3$) hydrated proton cluster ions. H⁺(H₂O)_n and the benzyl radical are the most probable fragmentation products.

(4) The only observed intermediate state is S₁; T_n or S₀ are not involved in these processes.

(5) Cluster ion fragmentation is so prevalent in aromatic/polar solvent clusters because stable products (e.g., benzyl radical, solvated protons, etc.) are generated and because cluster ion geometry is different from neutral cluster geometry. Polar solvents have large gas phase basicities [(H₂O)₃H⁺, ...] and the Franck-Condon factor for the I←S₁ transition is not large for Δν = 0 vibrational excitation. The ion cluster is thus created in a highly excited vibrational state for (most likely) both the van der Waals intermolecular modes and the toluene intramolecular modes.

(6) Cluster reaction dynamics for toluene⁺(H₂O)₃ can be characterized. The reaction fragment (H₂O)₃H⁺ is generated through two separate pathways with generation times τ₁ < 60 ns and τ₂ = 480 ns. The reaction fragment toluene⁺(H₂O)₂ is generated with a single time constant τ₁ < 60. Fragmentation dynamics of other clusters are too fast to measure within our instrument response function of ca. 20 ns FWHM.

ACKNOWLEDGMENTS

We wish to thank Professor D. F. Kelley for extensive and informative discussions concerning the kinetics of the

observed processes. This work was supported in part by grants from The Office of Naval Research and the National Science Foundation.

¹(a) R. Nowak, J. A. Menapace, and E. R. Bernstein, *J. Chem. Phys.* **89**, 1309 (1988); (b) M. Schauer, K. Law, and E. R. Bernstein *ibid.* **82**, 726 (1985); **82**, 736 (1985); (c) K. S. Law and E. R. Bernstein, *ibid.* **82**, 2856 (1985); (d) J. Wanna and E. R. Bernstein, *ibid.* **84**, 927 (1986); (e) J. Wanna, J. A. Menapace, and E. R. Bernstein, *ibid.* **85**, 1795 (1986); (f) M. R. Nimlos, D. F. Kelley, and E. R. Bernstein, *J. Phys. Chem.* **93**, 643 (1989).

²(a) A. Amiray, U. Even, and J. Jortner, *J. Chem. Phys.* **75**, 2489 (1981); (b) D. F. Kelley and E. R. Bernstein, *J. Phys. Chem.* **90**, 5164 (1986); (c) M. R. Nimlos, M. A. Young, E. R. Bernstein, and D. F. Kelley, *J. Chem. Phys.* **91**, 5268 (1989); (d) M. Hineman, D. F. Kelley, and E. R. Bernstein, *ibid.* **96**, 4904 (1992).

³S. K. Kim, S. Li, and E. R. Bernstein, *J. Chem. Phys.* **95**, 3119 (1991); M. F. Hineman, G. H. Brucker, D. F. Kelley, E. R. Bernstein, *ibid.* (submitted); Q. Y. Shang and E. R. Bernstein, *ibid.* (accepted).

⁴S. K. Kim, S. C. Hsu, S. Li, and E. R. Bernstein, *J. Chem. Phys.* **95**, 3290 (1991).

⁵S. Li and E. R. Bernstein (unpublished results).

⁶(a) B. Brutschy, *J. Phys. Chem.* **94**, 8637 (1990); (b) B. Brutschy, C. Janes, and J. Eggert, *Ber. Bunsenges. Phys. Chem.* **92**, 74 (1988).

⁷(a) A. J. Gotch, A. W. Garrett, D. L. Severance, and T. S. Zwier, *Chem. Phys. Lett.* **178**, 121 (1991); (b) A. J. Gotch and T. S. Zwier, *J. Chem. Phys.* **96**, 3388 (1992); (c) A. W. Garrett and T. S. Zwier, *ibid.* **96**, 3402 (1992).

⁸(a) S. Li and E. R. Bernstein, *J. Chem. Phys.* **97**, 804 (1992); following paper; (b) S. Li and E. R. Bernstein, *ibid.* (to be submitted, 1992).

⁹E. R. Bernstein, K. Law, and M. Schauer, *J. Chem. Phys.* **80**, 207 (1984).

¹⁰(a) K. S. Law and E. R. Bernstein, *J. Chem. Phys.* **82**, 2856 (1985); (b) M. Schauer, K. S. Law, and E. R. Bernstein, *ibid.* **81**, 49 (1984); (c) E. R. Bernstein, K. S. Law, and M. Schauer, *ibid.* **80**, 634 (1984).

¹¹J. L. Durant, D. M. Rider, S. L. Anderson, F. D. Proch, and R. N. Zare, *J. Chem. Phys.* **80**, 1817 (1984).